LANGMUIR

Article

pubs.acs.org/Langmuir

Adsorption Behavior of Low-Concentration Imidazolium-Based Ionic Liquid Surfactant on Silica Nanoparticles

Yan Liu,* Longjiao Qiao, Yinping Xiang, and Rong Guo*

School of Chemistry and Chemical Engineering, Yangzhou University, Yangzhou 225002, Jiangsu P. R. China

ABSTRACT: The adsorption behavior of imidazolium-based ionic liquid surfactant ([C_{12}mim]Br) on silica nanoparticles (NPs) has been studied with turbidity, isothermal titration microcalorimetry, fluorescence spectroscopy, and dynamic light scattering (DLS) measurements. Both the electrostatic attraction and the hydrogen bonding interaction between silica NP and [C_{12}mim]Br play crucial roles during [C_{12}mim]Br monomers binding to silica NPs at low surfactant concentration, and the hydrophobic effect leads to formation of micelle-like aggregates on silica NP surfaces with the further increase of surfactant concentration. Furthermore, it is found that sodium halide salts favor the adsorption of [C_{12}mim]Br on silica NP surfaces by decreasing the electrostatic repulsions. Anions with more hydrophobicity and the ability to form hydrogen bonding have more pronounced effect. Compared with DTAB, [C_{12}mim]Br has much stronger binding ability with silica NPs at pH 7.0. More interestingly, [C_{12}mim]Br can still form micelle-like aggregates on silica NP surfaces, but DTAB cannot at pH 2.0. The hydrogen bonding between the imidazolium ring and silica NPs is the principal contributor to these observations. Our results will contribute to the elucidation of silica NP/cationic surfactant interaction from molecular scale and the widely applications of silica NP/surfactant systems in practice.

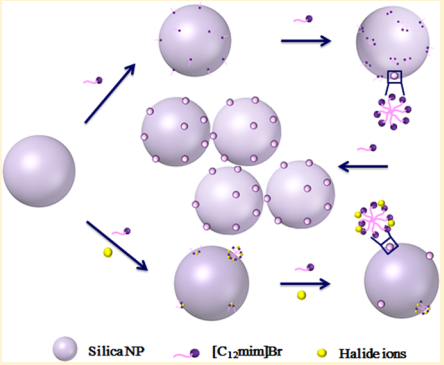

INTRODUCTION

Because of their unique and distinct characteristics, nanoparticles have important applications in the fields of medicine, electronics, optics, communications, energy, environment, etc.[1−3] Many of these applications require the adjoining of nanoparticles with surfactants, so interactions between nanoparticles and surfactants have attracted much interest.[4−6] Modifications in the physicochemical properties of nanoparticles upon the addition of surfactant will expand and enhance the overall capabilities and applications of the nanoparticle−surfactant mixtures.[7,8] The adsorption of surfactants on the nanoparticle surface is a cumulative effect of a number of forces such as the electrostatic force, covalent bonding, hydrogen bonding, hydrophobic effects, and so forth.[9−11] The interaction of nanoparticles and surfactants strongly depends on the characteristics of both nanoparticles and surfactants (type, charge, shape, size, etc.) as well as the environmental conditions used.[12−15] Thus, the nanoparticle−surfactant interaction is complex and specific, and more investigation from molecular levels is needed.

The behavior of adsorbed nonionic surfactants and the structure of their aggregates on silica NP surfaces have been widely investigated.[16−18] There are two different models discussed in the literature for the adsorption of nonionic surfactants considering bilayer formation or individual micelles decorating silica NPs. Recent studies have shown that micelle decoration on a nanoparticle surface is preferred because of an effective packing of hydrophobic tails for micelles as compared to that for bilayers.[16,17] Because of the formation of precipitate easily, the adsorption of cationic surfactants onto silica NP surfaces has been less studied. Although some earlier studies have to some extent indicated the micelle-like aggregate of cationic surfactant on silica NP surfaces,[14] there have been no attempts at directly experimentally estimating the strength and nature of these interactions. More detailed studies are needed to unequivocally demonstrate the nature of these interactions and their dependence on cationic surfactant structure.

Recently, 1-alkyl-3-methylimidazolium ionic liquids (ILs) with a long-chain substituent have attracted a great deal of attention due to their potential in various biological and pharmaceutical applications.[19−23] Compared with conventional ammonium surfactants, the ionic liquid surfactants display some advantages due to the existence of cationic imidazolium head groups. For example, the surface activity of surfactive imidazolium IL is somewhat better than that of conventional ionic surfactants, and they would exhibit significantly stronger tendency for self-aggregation.[24] This is due to the delocalized positive charge on the imidazolium ring and the ubiquitous hydrogen bonds among the imidazolium cations.[25,26] Then, what about the interaction between silica NPs and surfactive imidazolium ILs?

In the present work, we have carried out a detailed physicochemical investigation about the absorption behavior of imidazolium-based ionic liquid surfactant 1-dodecyl-3-methylimidazolium bromide ([C_{12}mim]Br) on the silica nanoparticles. It was found that the aggregation behavior of ionic liquid surfactant can be regulated and controlled by

Received: January 26, 2016
Published: February 28, 2016

DOI: 10.1021/acs.langmuir.6b00302
Langmuir 2016, 32, 2582−2590

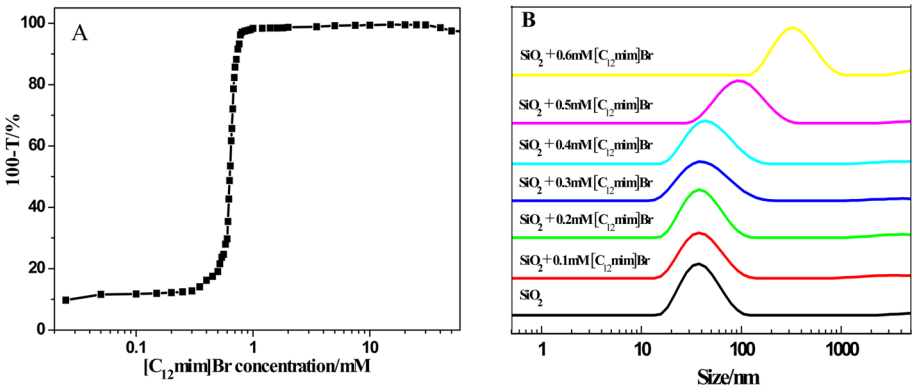

Figure 1. Turbidity (A) and size distribution functions (B) of silica NP/[C_{12}mim]Br systems with different [C_{12}mim]Br concentrations.

modulating pH, the alkyl chain length, and the addition of salt. For comparison, parallel measurements have also been made on the interaction between conventional ammonium surfactant dodecyltrimethylammonium bromide (DTAB) and silica nanoparticles. Based on these results, a detailed understanding of the nature of the adsorption and the specific stages of the micelle-like aggregate formation is given. This study provides new insights into the effect of headgroup on the binding of cationic surfactant to silica NP from the molecular level.

MATERIALS AND METHODS

Materials. An electrostatically stabilized colloidal suspension of silica particles, LUDOX TM-40 was obtained from Sigma-Aldrich. Dodecyltrimethylammonium bromide (DTAB, purity >99%) from Aldrich was recrystallized twice before use. Pyrene was obtained from Aldrich. Ionic liquids 1-alkyl-3-methylimidazolium bromide were synthesized according to a method previously described, and the purity was checked by ^{1}H NMR and FT-IR spectroscopy.[27,28] All other reagents used were of analytical grade, and distilled water was used. All samples were prepared in 5 mM sodium phosphate buffer at pH 6.8.

Turbidity Measurements. Turbidity measurements were carried out with a Shimadzu 1601 PC UV/vis spectrometer. The turbidity of the silica NP/IL mixed solutions was monitored by the transmittance at 450 nm. A cuvette with 1 cm pathway was used. All the measurements were conducted at 25 ± 0.1 °C.

Microcalorimetry. Heats of dilution were measured using a VP-ITC titration microcalorimeter from MicroCal Inc., Northampton, MA, at 25 ± 0.1 °C. Experiments were carried out titrating concentrated IL first into buffer and then into 0.5 wt % silica NP solution. In a typical experiment, silica NP solution was placed in the 1.438 cm^3 sample cell of the calorimeter, and [C_{12}mim]Br solution was loaded into the injection syringe. Both solutions were prepared in phosphate buffer and were degassed before use. [C_{12}mim]Br solution was titrated into the sample cell as a sequence of 50 injections of 5 × 10^{-6} dm^3 aliquots. The duration of each injection was 10 s, and the time delay (to allow equilibration) between successive injections was 240 s. The contents of the sample cell were stirred throughout the experiment at 307 rpm to ensure thorough mixing. Raw data were obtained as a plot of heating rate (μcal s^{-1}) against time (min). These raw data were then integrated to obtain a plot of observed enthalpy change per mole of injected [C_{12}mim]Br (ΔH_{obs}, kJ mol^{-1}) against [C_{12}mim]Br concentration (mM). Control experiments included the titration of [C_{12}mim]Br into buffer, buffer into silica NP solution, and buffer into buffer. The last two controls resulted in small and equal enthalpy changes for each successive injection of buffer and, therefore, will not be further considered in the data analysis.

Dynamic Light Scattering (DLS). Dynamic light scattering measurements were made at 25.0 ± 0.1 °C and at a scattering angle of 90° to the incident beam, using an ALV 5022 laser light-scattering instrument equipped with a 22 mW He−Ne laser at 632 nm (JDS model 1145P) in combination with an ALV-5000 digital correlator with a sampling time range of 1.0 μs−1000 ms. Experiment duration was in the range of 5−10 min, and each experiment was repeated two or more times.

Steady-State Fluorescence. Steady-state fluorescence experiments were performed with a RF-5301 luminescence spectrometer (Japan Shimadzu Company) equipped with a thermostated water-circulating bath. During the experiments, the excitation and emission slits were fixed at 3.0 and 1.5 nm, respectively, the excitation wavelength was set at 338 nm, and the emission spectra were collected from 350 to 500 nm. In all the measurements, the scan rate was selected at 240 nm/min. The intensity ratio of the first peak to the third peak (I_1/I_3) of the fluorescence spectrum of pyrene shows the microenvironmental polarity where the probe exists.[29,30]

RESULTS AND DISCUSSION

Adsorption Behavior of [C_{12}mim]Br on Silica NP Surfaces. We have first thoroughly characterized the LUDOX TM-40 particles using DLS, zeta potential, and TEM measurements. The TEM image indicates that these particles are approximately spherical, with an average particle diameter of around 22 nm (data not shown), in accordance with the manufacturer's specification. However, the particle size obtained by fitting the DLS data is larger than the TEM, possibly due to shrinkage of the particles during sample preparation for TEM imaging. The silica NPs have a zeta potential of −29.5 mV, indicating silica NP dispersions are electrostatically stabilized at pH 7.0.

Figure 1A shows the turbidimetric titration curve of silica NP solution with [C_{12}mim]Br. The turbidity begins to increase just over c_1 (0.5 mM) and then increases sharply to a maximum value at c_2 (0.9 mM) with the addition of [C_{12}mim]Br. Because the abrupt change of turbidity arises mainly from the change of the size and scattering factor of aggregates in the solution, the turbidity changes are supposed as the result of the formation silica NP/[C_{12}mim]Br aggregates. Above c_1, the adsorbed [C_{12}mim]Br leads to the aggregation of silica NPs and hence the increase of the turbidity of the system. Dynamic light scattering from the same system shows that the hydrodynamic size of the silica NP /[C_{12}mim]Br aggregates increases from about 35 to 80 nm when the [C_{12}mim]Br concentration increases to c_1 and then increases sharply with the further addition of [C_{12}mim]Br (Figure 1B).

Pyrene is one of the most popular fluorescent probes of polarity within organized media. Any change in the polarity of the microenvironment can be followed by studying the ratio of I_1/I_3 for pyrene, so insight into the adsorption behavior of [C_{12}mim]Br on silica NP surfaces can be obtained from fluorescence measurements. Figure 2 shows the dependence of

DOI: 10.1021/acs.langmuir.6b00302
Langmuir 2016, 32, 2582−2590

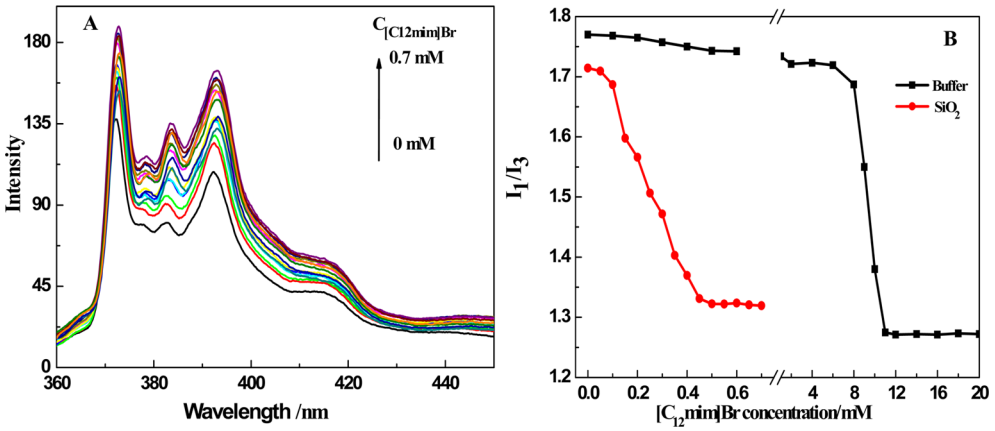

Figure 2. (A) Effect of $[C_{12}mim]Br$ on the fluorescence emission spectra of pyrene and (B) plots of I_1/I_3 of pyrene against $[C_{12}mim]Br$ concentration in the silica NP/$[C_{12}mim]Br$ system.

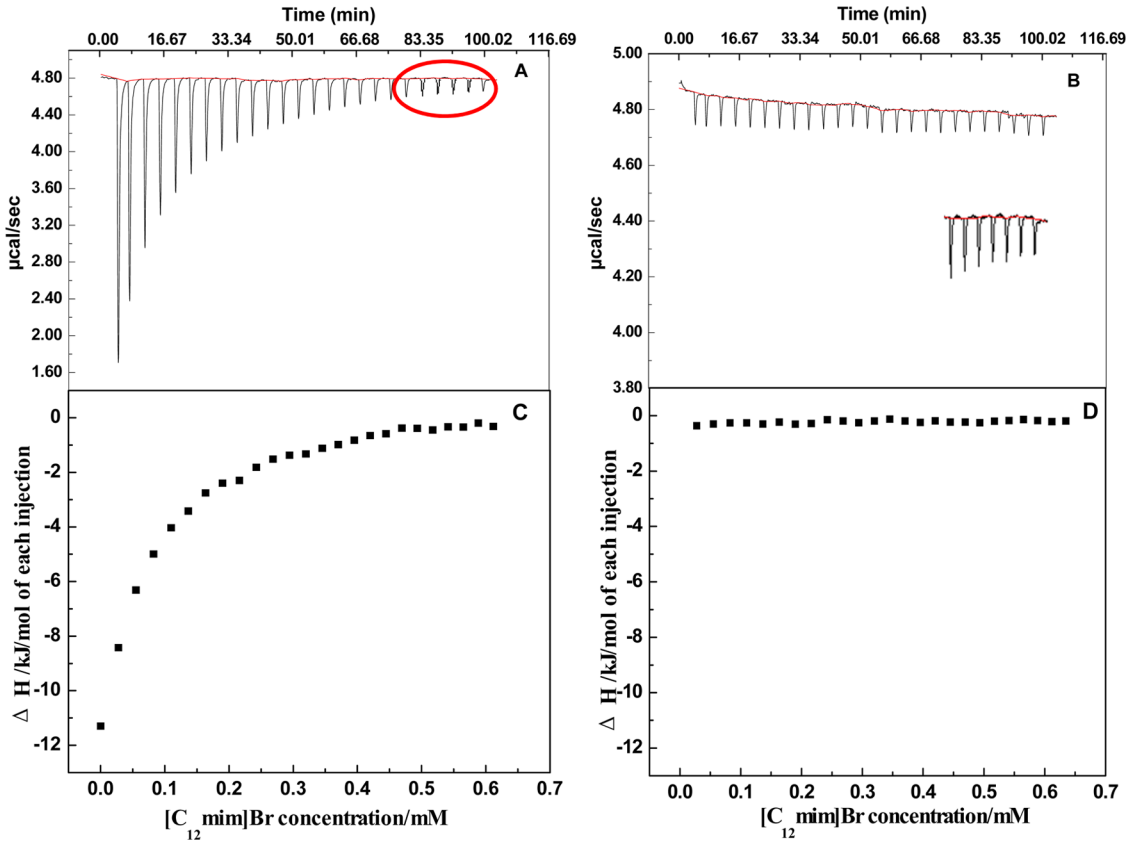

Figure 3. ITC curves of $[C_{12}mim]Br$ into silica NPs (0.5 wt %) (A, C) and buffer (B, D) solutions, at pH 7.0, $[C_{12}mim]Br$ concentration in the syringe being 4 mM. (A, B) Raw calorimetric data; (C, D) integrated data. The inset in (B) is the magnification of the circle area in (A).

the I_1/I_3 values on the IL concentration in the absence of and presence of silica NPs. As can be seen, the intensity ratio I_1/I_3 has a value of 1.71 in silica NP solution without $[C_{12}mim]Br$. I_1/I_3 here is a little lower than the value 1.77 when pyrene is dissolved in the pure water. This indicates the highly polar environment of pyrene molecules in contact with the surface silanol groups. In the absence of silica NPs, the sharp decrease of I_1/I_3 for the $[C_{12}mim]Br$ system with the increases of the surfactant concentration reflects the micellization of the surfactant. The similar change of I_1/I_3 is observed in the presence of silica NPs, and the I_1/I_3 values decreases sharply toward a plateau region at c_1 (0.5 mM). Moreover, I_1/I_3 for the silica NP/$[C_{12}mim]Br$ aggregates (1.32) is very similar to that for ordinary $[C_{12}mim]Br$ micelles (1.28). Therefore, micelle-like aggregates are formed on the silica NP surface above c_1 (0.5 mM) far below the critical micellar concentration (10 mM), in agreement with that obtained from the turbidity measurement. The addition of $[C_{12}mim]Br$ makes pyrene transfer to a more hydrophobic environment due to the formation of micelle-like aggregates on silica NP surfaces. The preference for micelle-like aggregates is a consequence of the high surface curvature of the silica NPs because an effective packing of hydrophobic tails is favored for micelles as compared to that for bilayers.[16,17]

At this stage, it is not clear just what kind of interaction leads to the binding of $[C_{12}mim]Br$ to silica NPs. The interaction between $[C_{12}mim]Br$ with silica NPs was studied more directly

DOI: 10.1021/acs.langmuir.6b00302
Langmuir 2016, 32, 2582−2590

using isothermal titration calorimetry (ITC). Figure 3 shows the ITC results for the [C_{12}mim]Br solutions being titrated into silica NP solutions and buffer solution against the final concentration of the IL. As shown in Figure 3B,D, the general large endothermic peak corresponding to the micelle dissociation is absent, and the enthalpy change is relatively small because it is only the result of [C_{12}mim]Br monomer dilution effects. Clearly, compared with the titration curves for the [C_{12}mim]Br solutions into the silica NP solution, the enthalpy change of the dilution curve can be neglected. However, in order to be more accurate, the enthalpy change after subtracting the dilution heat obtained from the titration of [C_{12}mim]Br in silica NP solution is shown in the following. As shown in Figure 3A,C, the enthalpy change in the ITC isotherms is highly exothermic upon the addition of [C_{12}mim]-Br, then decreases sharply, and finally reaches a small heat value with the continuous addition of [C_{12}mim]Br. The relatively strong exothermic is associated with the [C_{12}mim]Br−silica NP interaction. The association between a nanoparticles and oppositely charged surfactant is generally accepted as strong electrostatic attraction at low concentration. Thus, this exothermic enthalpy change is likely to caused by the binding of [C_{12}mim]Br monomers to negatively charged SiO^- groups on silica NPs surface upon the addition of [C_{12}mim]Br. Since the number of available binding sites on the surface of the silica NPs becomes progressively reduced during titration, the further increase of concentration leads to a sharp decrease in the measured exothermicity. Meanwhile, some neighborly bound [C_{12}mim]Br molecules may start to aggregate through hydrophobic effect. Above c_1, the individual surfactant monomers mainly bind to silica NPs via the hydrophobic effect with adsorbed [C_{12}mim]Br molecules. The transfer of the hydrophobic tail of [C_{12}mim]Br molecules from water into micelle-like aggregates would probably be exothermic, i.e., opposite to the endothermic enthalpy change associated with demicellization. However, the critical micelle-like aggregate concentration c_1 of [C_{12}mim]Br on silica NP surfaces could not be determined by the ITC method clearly. The reason may be due to a very dilute concentration of [C_{12}mim]Br. The endothermic enthalpy change associated with demicellization is high since the surfactant concentration is much larger than the concentration used here. Even so, we did observe a slightly exothermic enthalpy change above 0.5 mM [C_{12}mim]Br, which may be caused by the hydrophobic effect between the bound IL surfactants (inset in Figure 3B).

As is well-known, the imidazolium ring has the potential to form hydrogen bonding, so we postulated that the exothermic enthalpy change is also most likely due to hydrogen bonding between silanol groups on silica NP surfaces and the imidazolium ring of [C_{12}mim]Br. To verify this hypothesis, the effect of urea on the [C_{12}mim]Br and silica NP interaction was studied using ITC. Urea can disrupt existing hydrogen bonding by forming hydrogen bonding with all proton donors and acceptors. The enthalpy curves obtained from titrating 4 mM [C_{12}mim]Br into 0.5% silica NP solution in the absence and presence of 2 M urea are shown in Figure 4. As shown, the exothermic enthalpy change is still observable. However, the enthalpy change is significantly reduced from about −12.0 to −5.0 kJ/mol of each injection, and the [C_{12}mim]Br concentration required for achieving the constant low exothermic enthalpy change in the presence of urea (0.2 mM) is much lower than that in the absence of urea. This indicates that the extent of hydrogen bonding between the

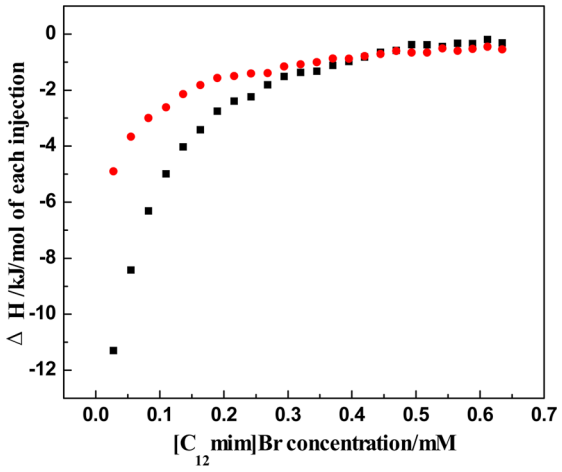

Figure 4. Enthalpy curves for titrating [C_{12}mim]Br into silica NPs (0.5 wt %)) in the absence of (square) and in the presence of 2 M urea (circle).

silanol groups on silica NP surfaces and [C_{12}mim]Br is weakened since most of the proton donating and accepting sites are occupied by urea molecules. Thus, both electrostatic attraction and hydrogen bonding play crucial role in the first adsorption of [C_{12}mim]Br molecules to silica NPs.

To confirm the role of the hydrophobic tail in the adsorption behavior of [C_{12}mim]Br on silica NP surfaces at higher concentration, we investigate the adsorption behavior of [C_4mim]Br and [C_8mim]Br on silica NP surfaces. For both [C_8mim]Br and [C_4mim]Br, the turbidity and I_1/I_3 against IL concentration curves show similar shape but much higher c_1 (Figure 5). The c_1 value increases sharply in the order [C_{12}mim]Br < [C_8mim]Br < [C_4mim]Br. Thus, the hydrophobic effect also matters much during the binding process of IL to silica NPs at higher IL concentration.

Effect of pH on the Adsorption Behavior of [C_{12}mim]Br on Silica NPs. Modifications of the silica NP surface by varying pH would change the density of SiO^- groups and therefore the interaction with surfactant. We further study the adsorption behavior of [C_{12}mim]Br on silica NP surfaces at different pH. The turbidity and fluorescence results for the [C_{12}mim]Br solution being titrated into silica NP solution at different pH are shown in Figure 6. At pH 2.0 and 11.0, both the turbidity and I_1/I_3 against [C_{12}mim]Br concentration show similar shape and tendency to the case at pH 7.0. The change tendency decreases in the order pH 11.0 > pH 7.0 > pH 2.0, so the binding interaction between [C_{12}mim]Br and silica NPs weakens in the order pH 11.0 > pH 7.0 > pH 2.0.

ITC was further employed to investigate the thermodynamic behavior associated with the interaction between silica NPs and [C_{12}mim]Br at different pH. Figure 7 shows the ITC curves for the concentrated [C_{12}mim]Br solutions being titrated into silica NP solutions against the final concentration of [C_{12}mim]Br at different pH. Compared with that at pH 7.0, a higher exothermic enthalpy change is observed for [C_{12}mim]Br titrating into silica NP solution upon the addition of [C_{12}mim]Br at pH 11.0. On the other hand, the ITC data at pH 2.0 show a significant reduced exothermic enthalpy change up the addition of [C_{12}mim]Br, which indicates that the interaction of [C_{12}mim]Br with silica NP at pH 2.0 is weak but still exists to the extent that considerable immobilization of [C_{12}mim]Br occurs under these conditions.

DOI: 10.1021/acs.langmuir.6b00302
Langmuir 2016, 32, 2582−2590

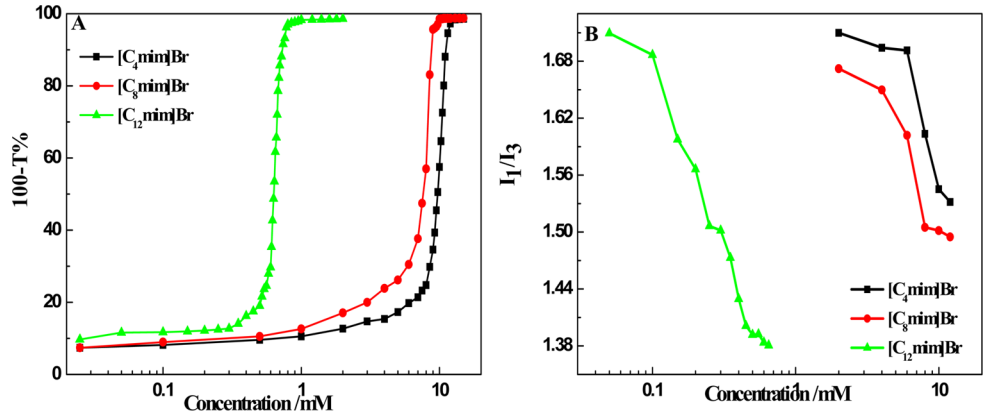

Figure 5. Turbidity (A) and I_1/I_3 (B) of silica NP/[$C_n$mim]Br systems against ionic liquid concentration.

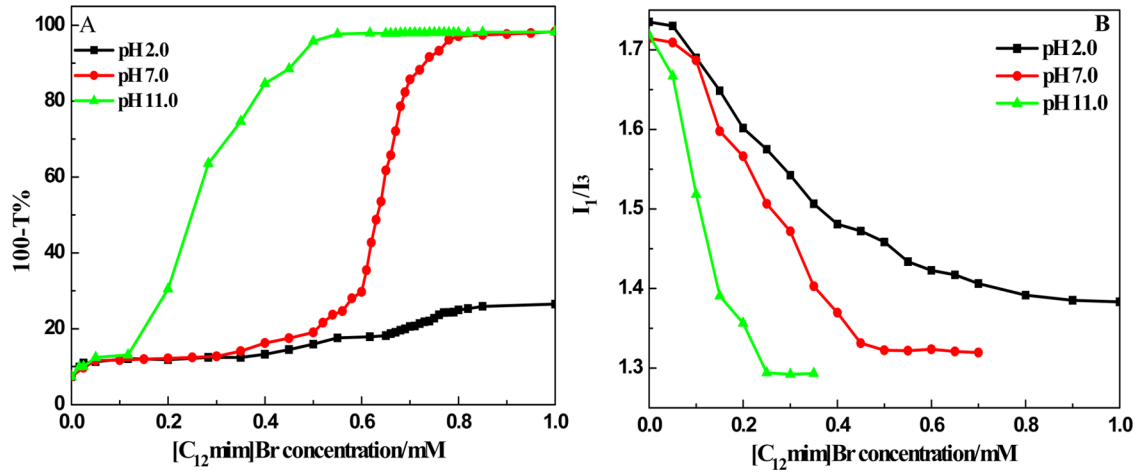

Figure 6. Turbidity of (A) and I_1/I_3 of pyrene in (B) silica NP/[C_{12}mim]Br systems against [C_{12}mim]Br concentration at different pH.

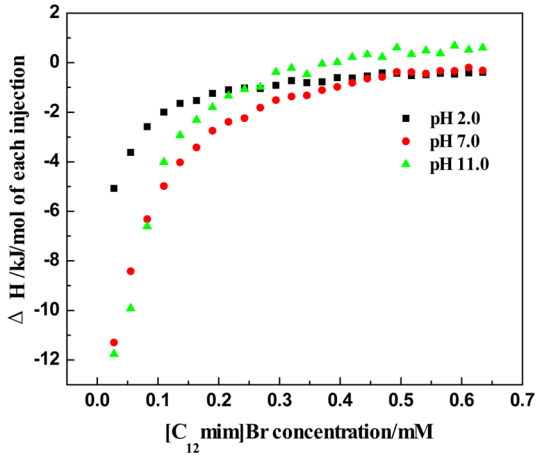

Figure 7. ITC curves of [C_{12}mim]Br titration into 0.5% silica NP solution at different pH.

The electrostatic attraction between [C_{12}mim]Br and silica NPs are stronger at pH 11.0 than that at pH 7.0, which increases the tendency of the [C_{12}mim]Br binding on NP surfaces, and hence a decreased c_1 value and higher exothermic enthalpy change. At pH 2.0, the silanol groups on silica NP surfaces are protonated effectively and thereby, not available for binding of [C_{12}mim]Br via electrostatic attraction. However, the silanol groups have a hydrogen donor as well as an acceptor, and they can readily form hydrogen bonding with the imidazolium ring. Therefore, the lower exothermic enthalpy change is most likely due to hydrogen bonding between the imidazolium ring of [C_{12}mim]Br and silica NPs. Because of the absence of electrostatic attraction, higher [C_{12}mim]Br concentration is needed to form micelle-like aggregates on silica NP surfaces and hence an increased c_1 value.

Effect of Inorganic Salt on the Adsorption Behavior of [C_{12}mim]Br on Silica NPs. Understanding of the specific salt effect on the aggregation behavior of ionic liquids surfactant on silica NP surfaces is relevant to multiple applications. Thus, the influence of a series of four salts (NaF, NaCl, NaBr, and NaI) on the aggregation behavior of [C_{12}mim]Br on silica NP surfaces has been further investigated. Figure 8 shows the turbidimetric titration curve of silica NP solution with [C_{12}mim]Br at 0.1 and 0.5 M salt. The c_1 value can be used to express the strength of interaction in the oppositely charged nanoparticle/surfactant system. Figure 9 shows the c_1 values for silica NP/[C_{12}mim]Br systems in the presence of different salts. For all the studied salts, the turbidimetric titration curve shows a faster increase in turbidity and a reduced c_1 in the presence of salt, indicating a stronger tendency for the [C_{12}mim]Br micelle-like aggregate formation on silica NP surfaces.

In our previous studies about negatively charged protein−[C_{12}mim]Br system, it is found that the addition of salt weakens the protein−[C_{12}mim]Br interaction, which is indicated by an increase in the critical aggregation concen-

DOI: 10.1021/acs.langmuir.6b00302
Langmuir 2016, 32, 2582−2590

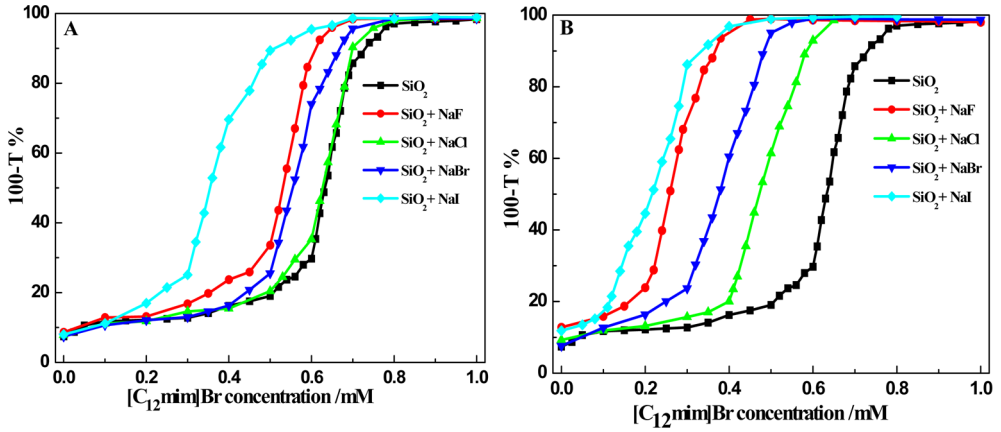

Figure 8. Turbidity of silica NP/[C_{12}mim]Br systems against [C_{12}mim]Br concentration in the presence of different salts.

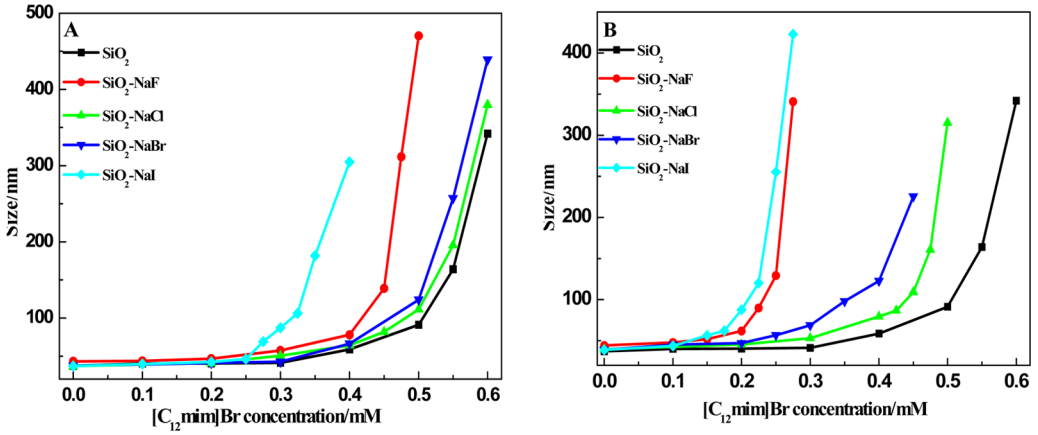

Figure 9. Size of silica NP/[C_{12}mim]Br systems against [C_{12}mim]Br concentration in the presence of different salts.

tration with increasing salt concentration.[30] Instead, the present results show that the critical aggregation concentration of IL surfactant on silica NP surfaces decreases after the addition of salt. Generally, the addition of salt to silica NP/[C_{12}mim]Br systems leads to two competing effects. On one hand, the addition of salt screens the electrostatic attraction between the oppositely charged silica NP surface and the surfactant molecule, which reduces the interaction between them. On the other hand, the addition of salt favors the formation of micelle-like aggregates on silica NP surfaces due to the screened electrostatic repulsion between surfactants. Here, the latter effect exceeds the former effect, resulting in a decrease of c_1 (Figure 10).

It can also be seen from Figure 10 that c_1 values decrease in the sequence: NaCl > NaBr > NaF > NaI at the constant salt concentration. In other words, the ability of the anions to promote aggregation of the IL was found to increase in the order NaCl < NaBr < NaF < NaI. Except for F^-, the effect of anions correlates well with the Hofmeister series,[31,32] and the trend observed for the c_1 of [C_{12}mim]Br on silica NP surfaces is actually analogous to those found for the critical micellar concentration of the conventional ionic surfactants such as dodecyltrimethylammonium bromide (DTAB) and [C_{12}mim]Br in aqueous solution.[33] The position of an anion in the Hofmeister series depends much on its charge and hydration radius. A larger hydration radius of the anions usually has a higher polarizability. A high polarizability enhances the binding of the anions at the surfactant aggregate surface and decreases

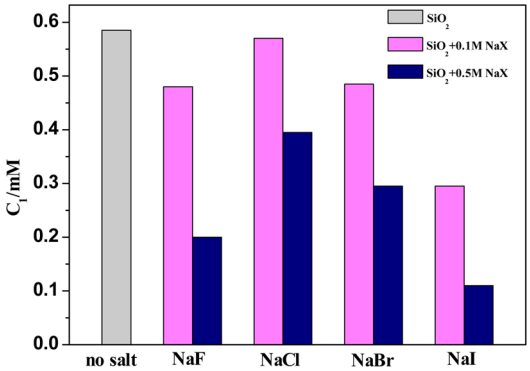

Figure 10. c_1 values of silica NP/[C_{12}mim]Br systems in the presence of different salts.

the electrostatic repulsion between the head groups of the surfactant, thus increasing the tendency of the [C_{12}mim]Br aggregation on silica NP surface and then lowering its c_1 value. Among the studied anions, the largest sized hydrophobic anions, I^-, is the most weakly hydrated and highly polarizable and can bind to the surface of the surfactant aggregates the most efficiently, which contributes to the formation of [C_{12}mim]Br micelle-like aggregates on silica NP surface and then the lowest c_1 value.

Surprisingly, F^- promotes the formation of micelle-like aggregates on silica NP surface more efficiently than Cl^- and Br^-. How can we understand the abnormal effect of F^- on the

DOI: 10.1021/acs.langmuir.6b00302
Langmuir 2016, 32, 2582−2590

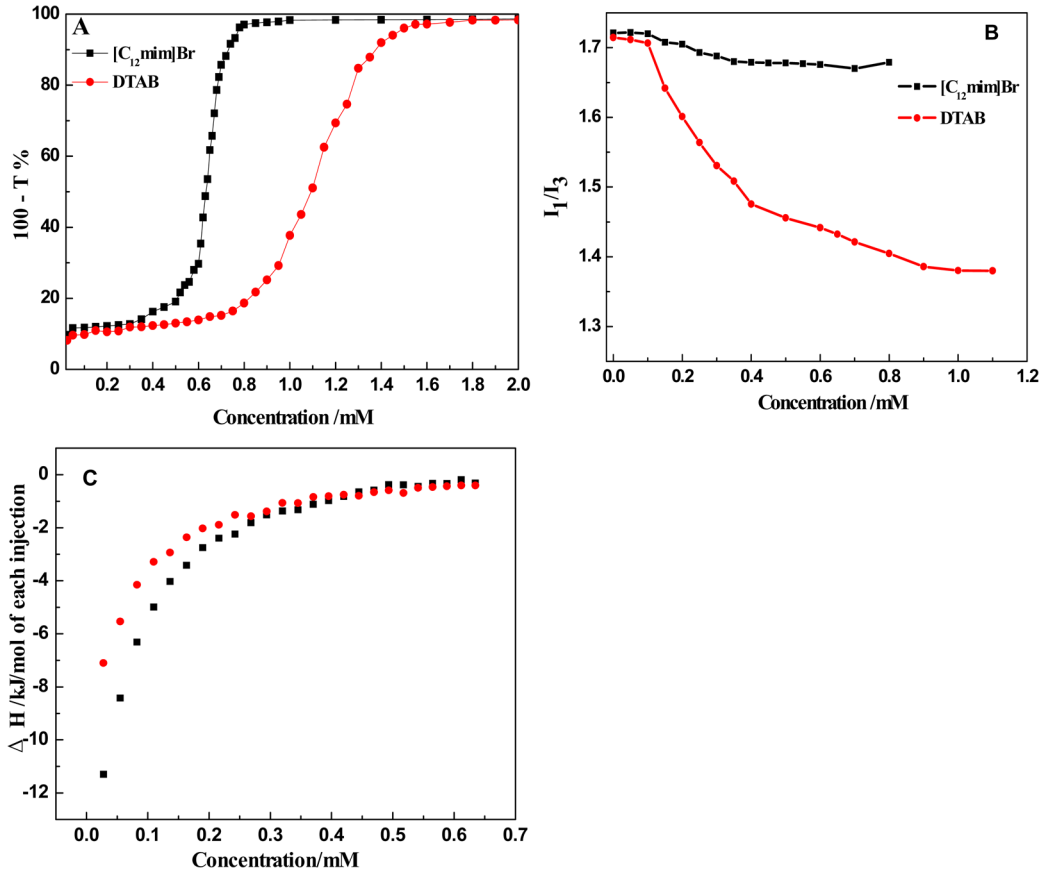

Figure 11. Turbidity (A), I_1/I_3 (B), and ITC curves (C) of silica NP/DTAB (circle) and silica NP/[C_{12}mim]Br (square) systems against surfactant concentration.

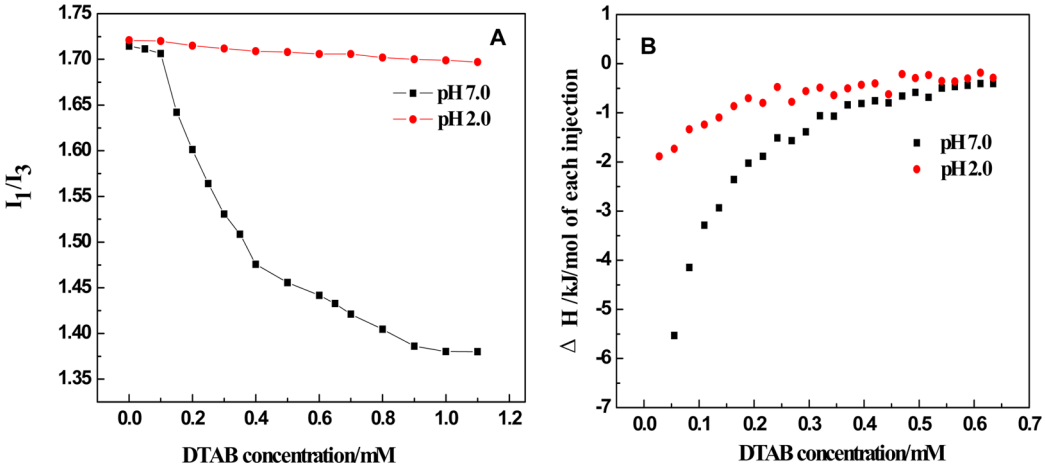

Figure 12. I_1/I_3 (A) and ITC curves (B) of silica NP/DTAB systems against surfactant concentration at pH 7.0 and 2.0.

absorption behavior of the IL on silica NP surface? Here, the hydration radius of F^- is the smallest, and F^- is the most highly hydrated and the least polarizable among the studied anions. As is well-known, F^- has the strong ability to form hydrogen bond. Thus, the abnormal effect of F^- may be attributed to the potency of hydrogen bond formation between F^- and silica NPs. The hydrogen bond effect enhances the binding of F^- to the surfactant micelle-like aggregate surface and promotes the formation of aggregates on silica NP surface.

Adsorption Behavior of DTAB on Silica NP Surfaces. To clarify the influence of the nature of the cationic ring on the silica NP−[C_{12}mim]Br interaction, a comparison was made between the silica NP interaction with [C_{12}mim]Br and its analogue conventional cationic surfactant, dodecyltrimethylammonium bromide (DTAB). The main reason for choosing DTAB is the presence of the same alkyl chain with that of [C_{12}mim]Br. For the silica NP/DTAB systems, the turbidity and fluorescence curves show similar shape and tendency to the silica NP/[C_{12}mim]Br systems. However, the variations in the turbidity observed in the silica NP/DTAB system are less significant than that in the silica NP/[C_{12}mim]Br system. The c_1 value for silica NP/DTAB (1.0 mM) obtained from the

DOI: 10.1021/acs.langmuir.6b00302
Langmuir 2016, 32, 2582−2590

turbidity and fluorescence results is higher than that for silica NP/[C_{12}mim]Br (0.5 mM) (Figure 11A,B). Therefore, the binding interaction between [C_{12}mim]Br and silica NPs should be stronger than that between DTAB and silica NPs. ITC titration curves for the DTAB solution being titrated into silica NP solution are shown in Figure 11C. For the silica NP/DTAB systems, the ITC curves show similar shape and tendency to the silica NP/[C_{12}mim]Br systems, and the lower exothermic ΔH_{obs} at the early stage of DTAB binding to silica NP is attributed to the weaker interaction between silica NP and DTAB.

All the above results demonstrate that the interaction between [C_{12}mim]Br and silica NP is stronger than that between silica NP and DTAB. Since [C_{12}mim]Br and DTAB have the same hydrophobic tail length, the interaction differences between the silica NP/[C_{12}mim]Br and silica NP/DTAB systems can be attributed to the different architectures of the cation. The nature of [C_{12}mim]$^+$−silica NP interactions appears to be significantly different from tetraalkylammonium cation−silica NP interactions. Compared with silica NP/DTAB, the electrostatic interactions between silica NP and [C_{12}mim]$^+$ are comparatively weaker due to the delocalization of the positive charge onto large imidazolium ring. Just as discussed above, considering the structure of [C_{12}mim]$^+$, the difference may be attributed to the potency of hydrogen bond formation, as well as $\pi-\pi$ interaction formation, which is lacking in DTAB.

For comparison, we also investigated the effect of pH on the adsorption behavior of DTAB on silica NP surfaces by fluorescence and ITC methods. As expected, similar to [C_{12}mim]Br, the adsorption of DTAB on silica NP surfaces is more effectively at pH 11.0 than that at pH 7.0 (data not shown). Interestingly, different adsorption behavior between DTAB and [C_{12}mim]Br is observed at pH 2.0. The fluorescence and ITC results for the DTAB solution being titrated into silica NP solution at pH 2.0 are shown in Figure 12. In contrast to [C_{12}mim]Br, neither obvious exothermic enthalpy change nor the decreased polarity of the added [C_{12}mim]Br was observed for the silica NP and [C_{12}mim]Br system due to the much lower driving force of DTAB binding compared to [C_{12}mim]Br. Evidently, for silica NP/DTAB system, the hydrogen bond between DTAB and silica NP is absent, so the interaction between them is very weak at pH 2.0. This leads to no obvious binding of DTAB on silica NP after addition of DTAB. The results clearly demonstrate that the imidazolium ring of the [C_{12}mim]Br has a pronounced effect on the adsorption behavior of [C_{12}mim]Br on silica surfaces at pH 2.0.

Binding Mechanism. On the basis of the above experimental evidence, a molecular mechanism of the interaction between silica NPs and [C_{12}mim]Br is proposed at pH 7.0, as shown schematically in Figure 13. The adsorption is driven primarily by electrostatic attraction and hydrogen bonding between the imidazolium ring of [C_{12}mim]Br and silica NPs, resulting in individual molecules binding on silica surfaces upon the addition of [C_{12}mim]Br. With the increase of [C_{12}mim]Br concentration, available binding sites on the surface of the silica NPs become progressively reduced. Meanwhile, some neighborly bound [C_{12}mim]Br molecules may start to aggregate through hydrophobic effect. However, the surfactant aggregates on silica NP surface have not yet become completely micelle-like at this moment. With the further increase of [C_{12}mim]Br concentration, the individual surfactant monomers bind to silica NPs via the hydrophobic effect with adsorbed [C_{12}mim]Br molecules, and micelle-like aggregates are formed on silica NP surfaces above c_1. The strong attraction between silica NPs and micelle-like aggregates leads to the aggregation of silica NPs and hence the increase of the turbidity of the system. Notably, our work indicates clearly that the micelle-like aggregates is built from isolated molecules from the aqueous solution and not by direct adsorption of micelles.

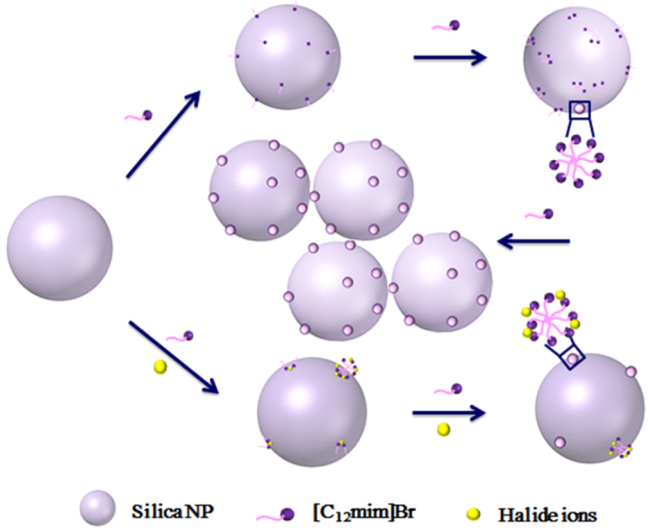

Figure 13. Schematic diagram describing the binding interactions between silica nanoparticles and [C_{12}mim]Br at different IL concentrations without (up) and with (down) salt.

Compared with the case at pH 7.0, the electrostatic attraction between [C_{12}mim]Br and silica NPs is stronger at pH 11.0 than that at pH 7.0, which increases the tendency of the [C_{12}mim]Br aggregation on NP surfaces and decreases its c_1 value. At pH 2.0, although the electrostatic attraction between silica NPs and [C_{12}mim]Br is reduced much, the hydrogen bonding can still lead to the formation of [C_{12}mim]Br aggregation on nanoparticle surfaces. The addition of salt favors the formation of micelle-like aggregates on silica NP surfaces due to the screened electrostatic repulsion between surfactants (Figure 13). Anions with more hydrophobicity and the ability to form hydrogen bonding have a more pronounced effect.

CONCLUSION

The adsorption behavior of imidazolium-based ionic liquid surfactant ([C_{12}mim]Br) on silica NP surfaces has been studied using various techniques. Especially, the present calorimetric investigation provided a detail view of the processes of [C_{12}mim]Br interaction with silica NPs at low surfactant concentration. It is revealed that both the electrostatic attraction and the hydrogen bonding interaction between silica NP and [C_{12}mim]Br play important roles during [C_{12}mim]Br monomers binding to silica NPs at low surfactant concentration. With the further increase of surfactant concentration, hydrophobic effect leads to formation of micelle-like aggregates on silica NP surfaces. Furthermore, the nature of interactions in silica NP/[C_{12}mim]Br system is different as compared with the silica NP/DTAB system, which is due to the hydrogen bonding between silica NP and [C_{12}mim]Br. Furthermore, the adsorption behavior of [C_{12}mim]Br on silica NPs can be regulated by the addition of inorganic salts. The stronger

DOI: 10.1021/acs.langmuir.6b00302
Langmuir 2016, 32, 2582−2590

hydrophobicity and the ability to form hydrogen bond of anions enhances their binding on the silica NP surface and promotes the formation of surfactant micelle-like aggregates on silica NP surfaces more effectively.

AUTHOR INFORMATION

Corresponding Authors

*Tel +86-514-87971802, Fax +86-514-87311374, e-mail yanliu@yzu.edu.cn (Y.L.).

*Tel +86-514-87971802, Fax +86-514-87311374, e-mail guorong@yzu.edu.cn (R.G.).

Notes

The authors declare no competing financial interest.

ACKNOWLEDGMENTS

This work was supported by the National Nature Science Foundations of China (21173182, 21573190), PAPD, and Nature Science Key Basic Research of Jiangsu Province for Higher Education (15KJA150009).

REFERENCES

(1) Dykman, L. A.; Khlebtsov, N. G. *Chem. Rev.* **2014**, *114*, 1258−1288.

(2) Cho, E. J.; Holback, H.; Liu, K. C.; Abouelmagd, S. A.; Park, J.; Yeo, Y. *Mol. Pharmaceutics* **2013**, *10*, 2093−2110.

(3) Neoh, K. G.; Kang, E. T. *Soft Matter* **2012**, *8*, 2057−2069.

(4) Mehan, S.; Chinchalikar, A. J.; Kumar, S.; Aswal, V. K.; Schweins, R. *Langmuir* **2013**, *29*, 11290−11299.

(5) Walker, J. M.; Gou, L.; Bhattacharyya, S.; Lindahl, S. E.; Zaleski, J. M. *Chem. Mater.* **2011**, *23*, 5275−5281.

(6) Binks, B. P.; Rodrigues, J. A. *Langmuir* **2007**, *23*, 3626−3636.

(7) Wang, Y.; Aili, D.; Selegård, R.; Tay, Y.; Baltzer, L.; Zhang, H.; Liedberg, B. *J. Mater. Chem.* **2012**, *22*, 20368−20373.

(8) Fernández-Rodríguez, M. A.; Rodríguez-Valverde, M. A.; Cabrerizo-Vílcheza, M.; Hidalgo-Alvarez, R. *Soft Matter* **2014**, *10*, 3471−3476.

(9) Mehan, S.; Aswal, V. K.; Kohlbrecher, J. *Langmuir* **2014**, *30*, 9941−9950.

(10) Grant, L. M.; Tiberg, F.; Ducker, W. A. *J. Phys. Chem. B* **1998**, *102*, 4288−4294.

(11) Mu, Q.; Jiang, G.; Chen, L.; Zhou, H.; Fourches, D.; Tropsha, A.; Yan, B. *Chem. Rev.* **2014**, *114*, 7740−7781.

(12) Lugo, D. M.; Oberdisse, J.; Lapp, A.; Findenegg, G. H. *J. Phys. Chem. B* **2010**, *114*, 4183−4191.

(13) Bharti, B.; Meissner, J.; Gasserb, U.; Findenegg, G. H. *Soft Matter* **2012**, *8*, 6573−6581.

(14) Kumar, S.; Aswal, V. K.; Kohlbrecher, J. *Langmuir* **2012**, *28*, 9288−9297.

(15) Tyrode, E.; Rutland, M. W.; Bain, C. D. *J. Am. Chem. Soc.* **2008**, *130*, 17434−17445.

(16) Lugo, D.; Oberdisse, J.; Karg, M.; Schweins, R.; Findenegg, G. *Soft Matter* **2009**, *5*, 2928−2936.

(17) Sharma, K. P.; Aswal, V. K.; Kumaraswamy, G. *J. Phys. Chem. B* **2010**, *114*, 10986−10994.

(18) Sarkar, B.; Venugopal, V.; Tsianou, M.; Alexandridis, P. *Colloids Surf., A* **2013**, *422*, 155−164.

(19) Menger, F. M.; Keiper, J. S. *Angew. Chem., Int. Ed.* **2000**, *39*, 1906−1920.

(20) Ohno, H.; Suzuki, C.; Fukumoto, K.; Yoshizawa, M.; Fujita, K. *Chem. Lett.* **2003**, *32*, 450−451.

(21) Baker, S. N.; McCleskey, T. M.; Pandey, S.; Baker, G. A. *Chem. Commun.* **2004**, 940−941.

(22) De Diego, T.; Lozano, P.; Gmouh, S.; Vaultier, M.; Iborra, J. L. *Biomacromolecules* **2005**, *6*, 1457−1464.

(23) Fujita, K.; MacFarlane, D. R.; Forsyth, M.; Yoshizawa-Fujita, M.; Murata, K.; Nakamura, N.; Ohno, H. *Biomacromolecules* **2007**, *8*, 2080−2086.

(24) Dong, B.; Li, N.; Zheng, L.; Yu, L.; Inoue, T. *Langmuir* **2007**, *23*, 4178−4182.

(25) Miki, K.; Westh, P.; Nishikawa, K.; Koga, Y. *J. Phys. Chem. B* **2005**, *109*, 9014−9019.

(26) Zhang, H. C.; Li, K.; Liang, H.; Wang, J. *Colloids Surf., A* **2008**, *329*, 75−81.

(27) Holbrey, J. D.; Seddon, K. R. *J. Chem. Soc., Dalton Trans.* **1999**, 2133−2140.

(28) Baltazar, Q. Q.; Chandawalla, J.; Anderson, J. L. *Colloids Surf., A* **2007**, *302*, 150−156.

(29) Lianos, P.; Viriot, M. L.; Zana, R. *J. Phys. Chem.* **1984**, *88*, 1098−1101.

(30) Liu, Y.; Guo, R. *Biomacromolecules* **2007**, *8*, 2902−2908.

(31) Anacker, E. W.; Ghose, H. M. *J. Am. Chem. Soc.* **1968**, *90*, 3161−3166.

(32) Larsen, J. W.; Magidl, L. J. *J. Am. Chem. Soc.* **1974**, *96*, 5774−5782.

(33) Wang, H.; Feng, Q.; Wang, J.; Zhang, H. *J. Phys. Chem. B* **2010**, *114*, 1380−1387.

DOI: 10.1021/acs.langmuir.6b00302
Langmuir 2016, 32, 2582−2590